Article

Design and Fabrication of a Novel Hybrid-Structure Heat Pipe for a Concentrator Photovoltaic

Hsin-Jung Huang, Sheng-Chih Shen * and Heiu-Jou Shaw

Department of Systems and Naval Mechatronic Engineering, Research Center for Energy Technology and Strategy, National Cheng Kung University, No.1, University Road, Tainan 701, Taiwan; E-Mails: p1897104@mail.ncku.edu.tw (H.-J.H.); nmshaw@mail.ncku.edu.tw (H.-J.S.)

* Author to whom correspondence should be addressed; E-Mail: scshen@mail.ncku.edu.tw; Tel.: +886-6-2747018; Fax: +886-6-2747019.

Abstract: This study presents a design method to fabricate a novel hybrid-structure flat plate heat pipe (NHSP heat pipe) for a concentrator photovoltaic. The NHSP heat pipe is composed of a flattened copper pipe and a sintered wick structure, and a coronary-stent-like rhombic copper mesh supports the structure. The coronary-stent-like supporting structure enhances the mechanical strength and shortens the reflux path of the working fluid. Experiments demonstrate that the sintered capillary heat pipe reduces the thermal resistance by approximately 72%, compared to a traditional copper mesh-screen heat pipe. Furthermore, it can reduce thermal resistance by 65% after a supporting structure is added to the heat pipe. The results show that the NHSP heat pipe provided the best performance for the concentrator photovoltaic, which can increase photoelectric conversion efficiency by approximately 3.1%, compared to an aluminum substrate.

Keywords: Biot number; tubular; heat pipe; concentration photovoltaic (CPV)

1. Introduction

In recent years, the development of renewable energy sources, including solar energy, wind power, and biodiesel, has been viewed as a method of reducing greenhouse gases. Among these energy sources, solar energy is the most stable when generating power. For all types of solar energy, III-V solar cells (InGaP/GaAs/Ge) and high-concentration photovoltaic (HCPV) have the highest

efficiency—approximately 36%–40%. Numerous methods have been used to increase the conversion efficiency of HCPV [1–3]. Despite its high efficiency in all types of solar cells, 60%–64% of collected solar energy is transformed into heat rather than electricity. However, the efficiency of HCPV is reduced by 0.2% to 0.5% for every temperature rise of 1 °C [4]. Temperature is the most critical factor affecting the efficiency of solar cells, especially III-V solar cells. Furthermore, the HCPV lifetime is highly dependent on operation temperature. Therefore, the design for heat dissipation plays an important role in concentrator photovoltaic modules [5,6], especially the passive cooling method, which is a cooling technology that does not consume power and has been used in various fields [7,8]. Therefore, when efficiently implemented, heat pipes play a critical role in passive cooling in the modern green energy industry.

Ming *et al.* [9] and Gillot *et al.* [10] studied flat plate heat pipes used for electronic cooling and analyzed their thermal resistances. In addition, they compared two wick structures, namely, sintered metal and groove types. Bai *et al.* [11] determined through experiments that the performances of heat pipes depend on the depth-to-width ratio of the groove structure. Furthermore, the porosity ratio of the sintered metal type must be increased, whereas the mesh number of the screen must be decreased or the layers of the mesh screen must be increased. This method enhances the capillary pumping of microstructures [12]. Lin *et al.* [13] presented a novel groove microstructure. Through experiments, the heat transfer coefficient at the condenser of this composite structure was discovered to be 120% higher than that of the traditional groove structure. Therefore, the composite structure compensates for the defects of the traditional structure. Using this concept, thermal management systems of HCPV cooling can be improved.

This study designs a batch process and a low thermal resistance for NHSP heat pipes, which comprises a flattened copper pipe shell, a sintered wick structure, and a newly designed supporting structure, hereafter referred to as the NHSP heat pipe. This study shows that the NHSP heat pipe increases the photovoltaic conversion efficiency of III-V type solar cells.

2. Design and Fabrication of the NHST Heat Pipe

Figure 1(a) shows the working mechanism and structure of the NHSP heat pipe, which consists of a flattened copper pipe shell, a sintered wick structure, a coronary-stent-like supporting structure, and a working fluid. Figure 1(b) shows a diagram of the coronary-stent-like supporting structure. A rhombic copper mesh was stamped by a pre-shaped mold, and the short reflux paths of the working fluid were extended from the heat source in different directions. At one end of the NHSP heat pipe was the evaporation section, which absorbed heat by contacting the heat source. At the opposite end was the condensation section, through which absorbed heat is dissipated into the surrounding environment. The working fluid in the evaporation section is heated and boiled, and the vapor gradually fills the interior space of the NHSP heat pipe. Thereafter, the vapor condenses in the condensation section where the temperature is decreased, and then the working fluid flows back to the evaporation section through the wick and supporting structures. Therefore, the reciprocal cycle is completed.

Figure 1. Working mechanism and supporting structure of the NHST heat pipe.

(**a**) Mechanism of heat pipe   (**b**) Supporting structure of NHSP heat pipe
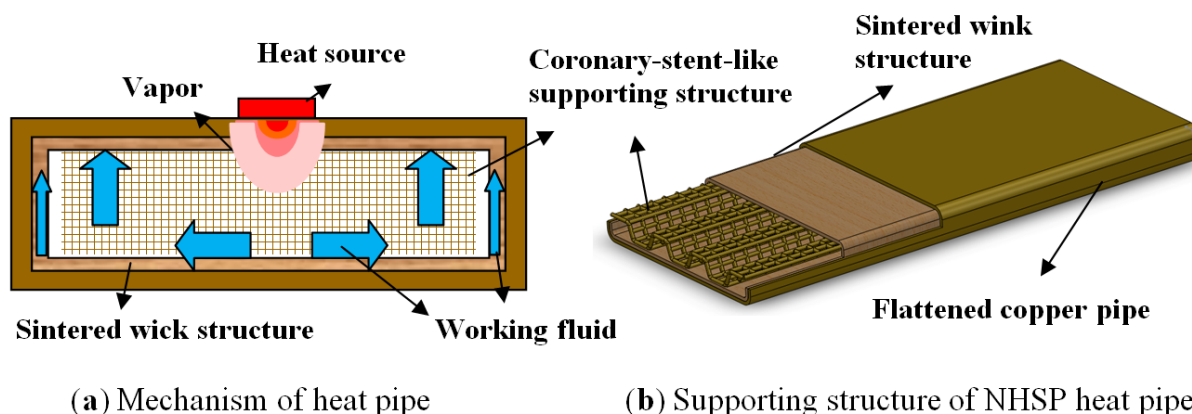
For common flat plate heat pipes without any supporting structure, their hollow chambers account for a large portion of their volume. Consequently, their mechanical strength is inferior to that of concrete metal substrates. The working fluid can flow back to the evaporation section only through the wick structure in the chamber, and the reflux path of the fluid is long. Therefore, the thermal resistance is high, and the problem of hot spots remains. Therefore, this study presents an NHSP heat pipe with primary components that include a flattened copper pipe shell, a supporting structure, a sintered wick structure, and working fluid. The sintered wick structure improves the boiling heat transfer process. In addition, the coronary-stent-like supporting structure enhances the mechanical strength of the heat pipe, providing more diffusion paths for the vapor and shortening the reflux path of the working fluid. This hybrid structure, which combines these two basic structures, enhances the thermal performance of NHSP heat pipes. The fabrication method of the NHSP heat pipe is explained as follows: first, a hollow copper tube is constructed using the extrusion process. Thereafter, copper powder is placed in the remaining space between the mandrel and the inner wall. Next, sintering is conducted and the mandrel is removed, and the copper tube is stamped into a flattened pipe. Thereafter, the supporting structure is placed into a flattened copper pipe. Subsequently, working fluid is injected through a filling hose into the heat pipe. Finally, the heat pipe is evacuated and sealed, and the fabrication process of the NHSP heat pipe is thus complete.

3. Thermal Performance Measurement

The measurement system included a wind tunnel, fan, pressure device, heat source, heat pipe, and heat sink [Figure 2(a)]. To simulate the conditions in South Taiwan in August, the fan had a steady wind velocity of 3.5 m/s. The evaporation and condensation sections of the heat pipe were in contact with the heat source and heat sink, respectively. The pressure device over the heat sink applied a fixed pressure (*i.e.*, approximately 60 lb according to the Intel standard) to ensure that the thermal contact resistance remained uniform throughout the thermal performance measurement. The heat source consisted of copper blocks (40 mm × 40 mm × 20 mm), in which there were two 150 W heating rods. Thereafter, the insulator was wrapped around the heat pipe, separating the copper block from the surrounding environment. Consequently, the total thermal loss was negligible, and the electric power was the approximate thermal power.

Figure 2. (a) NHST heat pipe measurement device; (b) distribution of the measurement points.

(a)

(b)
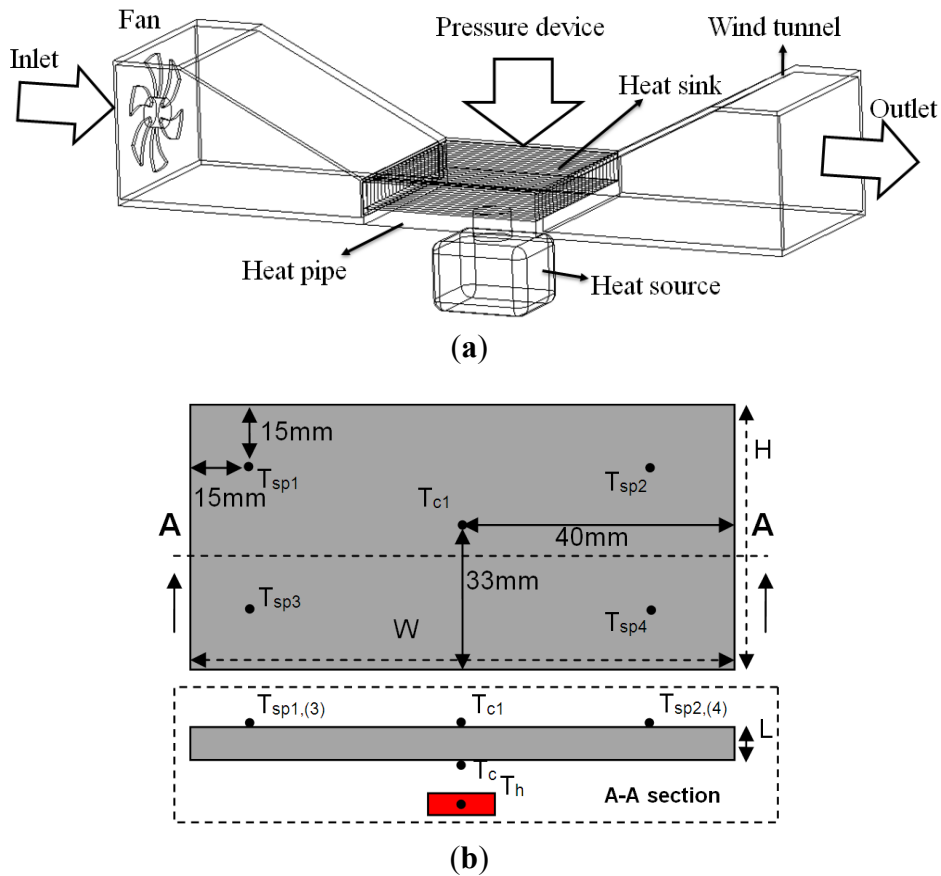
As shown in Figure 2(b), the distribution of the measurement point T_h was the temperature point on the surface of the heater, T_c was the central temperature point of the evaporation section, T_{c1} was the central temperature point of the condensation section, and points T_{sp1} to T_{sp4} were the temperature points on the edge of the heat pipe. T_{sp} was the arithmetic mean of T_{sp1} to T_{sp4}, and Q was the input power of the heat pipe:

$$R_{eff} = \frac{T_c - T_{c1}}{Q} \tag{1}$$

where R_{eff} was the total thermal resistance in the z direction (*i.e.*, thickness) of the heat pipe, including the wall surface, wick structure, phase change, and vapor flow thermal resistance. Therefore, the thermal resistance between the center of the evaporation section and the condensation section was defined in this experiment as the effective thermal resistance, which is expressed as follows:

$$R_{sp} = \frac{T_{c1} - T_{sp}}{Q} \tag{2}$$

where R_{sp} was the spreading resistance on the xy-plane or the condensation section. Therefore, the thermal resistance between the condensation section and the boarder point of the heat spreader was defined in this experiment as the thermal spreading resistance. The Biot number (Bi) was expressed in the following formula:

$$\text{Biot} = \frac{h_{eff} \times r}{K_{eff}} \tag{3}$$

$$h_{eff} = Q \big/ A\big(T_{sp} - T_{amb}\big) \tag{4}$$

$$K_{eff} = L \big/ AR_{eff} \tag{5}$$

where h_{eff} was the effective heat transfer coefficient applicable to the space between the heat pipe and the ambient, which can be expressed as (4); K_{eff} was the effective thermal conductivity coefficient of the NHSP heat pipe, which can be expressed as (5); r was the effective radius of the heat pipe, which can expressed as $W \times H/(W + H)$; A was the cross-section area of the heat pipe that equaled $W \times H$; and T_{amb} was the ambient temperature.

Bi is a dimensionless number that describes the distribution ratio of the internal to external thermal resistance of an object (in this case, the heat pipe). When the heat pipe size is fixed and the effective heat convection coefficient as namely, the external thermal resistance is unchanged and its thermal conductivity coefficient rises as the Bi decreases (*i.e.*, its internal thermal resistance decreases).

4. Results and Discussion of the Experiments

4.1. Experiments with Different Capillary Structures

Table 1 lists the production parameters of the sintered capillary heat pipe (Type 1) and the copper screen capillary heat pipe (Type 2). As shown in Figure 3(a), R_{sp} of the sintered capillary heat pipe was nearly equal to that of the copper screen capillary heat spreader, but R_{eff} of Type 1 was much lower than that of Type 2. When the input power reached 100 W, R_{eff} of Type 1 was 0.054 °C/W, whereas that of Type 2 was as high as 0.194 °C/W. As shown in Figure 3(b), the Bi of the sintered capillary heat pipe was smaller than that of the copper screen of the capillary heat pipe. When the effective heat convection coefficient (*i.e.*, external thermal resistance) remained constant, the thermal resistance of Type 1 was lower than that of Type 2.

Table 1. The production parameters of the heat pipes using different capillary structures.

	Sintered metal heat pipe (Type 1)	Copper mesh screen heat pipe (Type 2)
Specifications	80 mm × 65 mm × 4.0 mm (length × width × depth)	80 mm × 65 mm × 4.0 mm (length × width × depth)
Working Fluid	pure water	pure water
Capillary Structure	100-200-mesh sintered copper powder	270-mesh copper screen
Thickness of Capillary Structure	0.35 mm	0.35 mm
Supporting Structure Specifications	72 mm × 60 mm × 1.7 mm (rhombic multi-hole copper screen)	72 mm × 60 mm × 1.7 mm (rhombic multi-hole copper screen)

Figure 3. (**a**) R_{eff} and R_{sp} of the two heat pipes changing with the input power; (**b**) Thermal resistances of the two heat pipes changing with the Biot number (Bi).

(**a**)   (**b**)
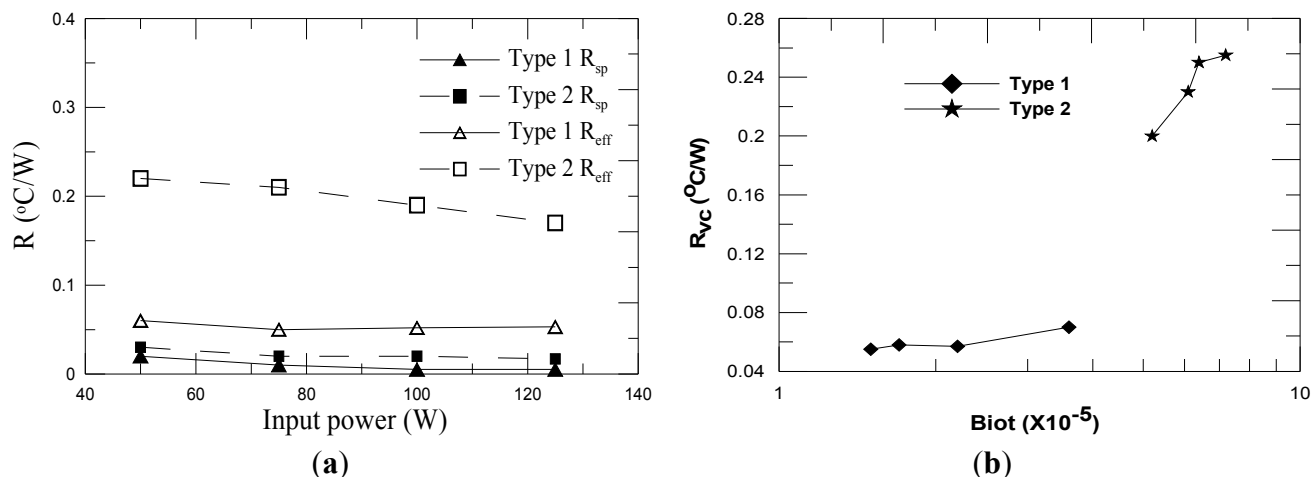
According to the experimental results, the thermal resistance of the sintered capillary heat pipe is evidently much lower than that of the copper mesh screen capillary heat pipe and behaves like Bi. The result is determined by the features of the sintered metal heat pipe, which can be used for the concentrator photovoltaic with high heat flux density. Furthermore, because its thermal resistance is low, it is helpful to address the problem arising from hot spots caused by the concentrator photovoltaic.

4.2. Experiments on the Effects of the Coronary-Stent-Like Supporting Structure

Table 2 shows the production parameters of the heat pipe with (Type 3) or without (Type 4) the supporting structure.

Table 2. The production parameters of the heat pipes using different capillary structures.

	With supporting structure (Type 3)	Without supporting structure (Type 4)
Specifications	80mm × 65mm × 4.0mm (length × width × depth)	80mm × 65mm × 4.0mm (length × width × depth)
Working Fluid	pure water	pure water
Capillary Structure	100-200-mesh sintered copper powder	100-200-mesh sintered copper powder
Thickness of Capillary Structure	0.3mm	0.3mm
Supporting Structure Specifications	72mm × 60mm × 1.7mm (rhombic multi-hole copper screen)	Unavailable

As shown in Figure 4(a), R_{sp} of the Type 3 heat pipe was nearly equal to that of Type 4 when the input power exceeded 100 W. In addition, when the input power was 100 W, the difference between them was approximately 0.02 °C/W, which was negligible. However, R_{eff} of the Type 3 heat pipe was much lower than that of Type 4. With a 100 W input power, R_{eff} of the Type 3 heat pipe was 0.060 °C/W, whereas that of Type 4 was as high as 0.144 °C/W. As shown in Figure 4(b), the Bi of the Type 3 heat pipe was smaller than that of Type 4. When the effective heat convection coefficient (*i.e.*, external thermal resistance) was fixed, the thermal resistance of the Type 3 heat pipe was less than that of Type 4.

According to these results, there was no significant difference in thermal spreading resistance (*i.e.*, R_{sp} between the Type 3 heat pipe and that of Type 4), but there was a significant difference in effective thermal resistance (*i.e.*, R_{eff}). This result was caused by the supporting structure, which helped enhance the mechanical strength and shortened the reflux path of the condensed fluid. Consequently, the condensed fluid quickly returned to the evaporation section and removed the heat, decreasing the thermal resistance of the heat pipe.

Figure 4. (**a**) Effects of the supporting structure of the heat pipe on R_{eff} and R_{sp}; (**b**) thermal resistance of the heat pipe changing with the Biot number.


(**a**)

(**b**)
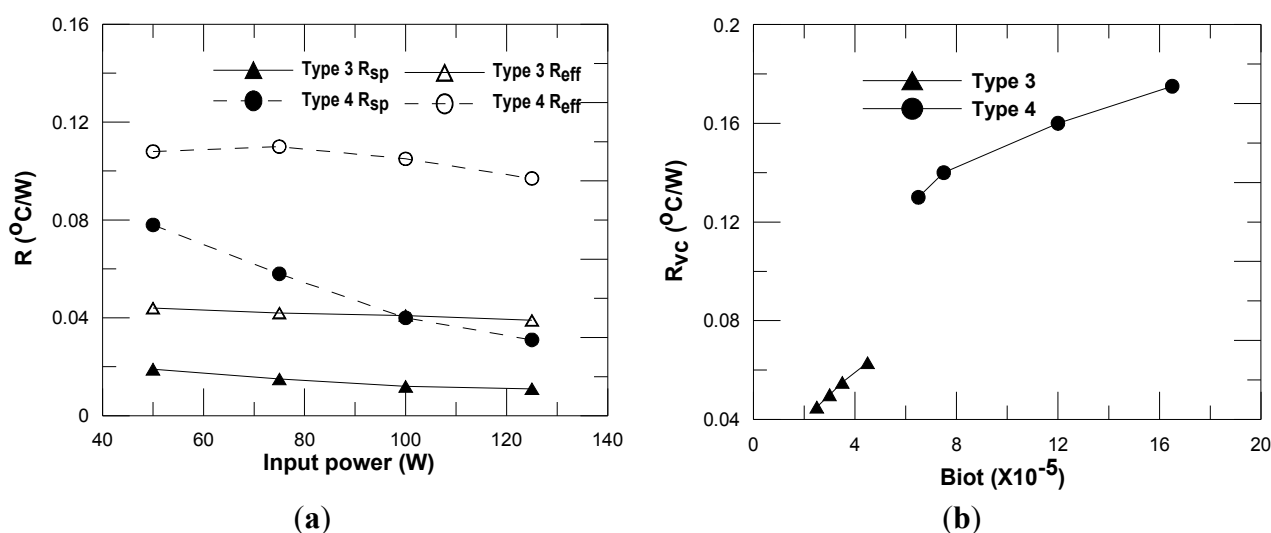
4.3. Measurement of Thermal Performance with Different Substrate Using HCPV

According to the experimental results, the NHSP heat pipe with sintered metal and a coronary-stent-like supporting structure had increased heat efficiency and a decreased temperature gradient. The design of the supporting structure reduced the spreading resistance, thereby increasing the thermal performance of the entire system. With its high heat dissipation and high heat flux, the NHSP heat pipe has superior performance. Following simulated experiments with a small-area heat source, a sun tracker was constructed (Figure 5) for an HCPV combined with three substrates. A 270 mm × 270 mm Fresnel lens was used as the concentrator to concentrate sunlight to a 10 mm × 10 mm area. The experiment was performed in South Taiwan in August 2011. The sun power was in the range of 900 to 930 W/m^2, the ambient temperature was approximately 35 °C, and the average wind velocity was approximately 3.1 m/s during the experiment. Therefore, nearly 40 W was concentrated on the cell if the efficiency of the lens was 60%. Figure 6 shows the P/V curves of the three cases. The NHSP heat pipe had the highest power, compared to the copper and aluminum substrates, because of its low junction temperature. The maximum power of the HCPV with the NHSP heat pipe, copper, and aluminum substrate was 4,406, 3,972, and 3,232 mW, respectively. The conversion efficiencies of the three cases were 11.2%, 9.9%, and 8.1%, respectively. Using the NHSP heat pipe as the solar module enhanced the efficiency by approximately 3.1% compared to the aluminum substrate in a single solar cell.

Figure 5. Constructed sun tracker.

Figure 6. P/V curve of solar cell with different substrates.
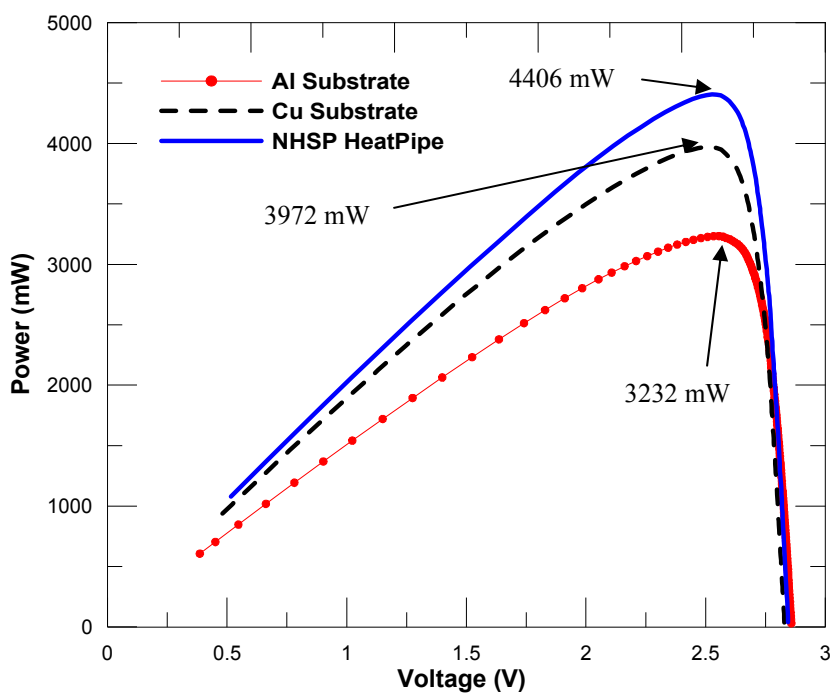
5. Conclusions

This study presented a novel NHSP heat pipe and investigated its thermal conductivity experimentally. First, the thermal performances of the sintered-metal structured heat pipe and the copper mesh capillary-structured heat pipe were compared, and the thermal resistance of the sintered-metal structure heat pipe was approximately 72% less than that of the copper mesh heat pipe. This result is attributable to the effective thermal conductivity of the heat pipe, that is, the features of the sintered capillary structure. As shown by the experiments, the thermal resistance of the heat pipe with the supporting structure was approximately 65% less than that of the heat pipe without a supporting structure. By combining the sintered capillary structure with the coronary-stent-like supporting structure, the NHSP heat pipe reduced its Bi and thermal resistance. Finally, this study used an HCPV as the heat source with various substrates to determine its thermal performance by comparing the power conversion efficiencies. The results showed that the NHSP heat pipe increased the HCPV conversion efficiency by approximately 3.1% in a single solar cell.

Acknowledgments

References

1. Lee, H.C.; Wu, S.C.; Yang, T.C.; Yen, T.J. Efficiently harvesting sun light for silicon solar cells through advanced optical couplers and a radial p-n junction structure. *Energies* **2010**, *3*, 784–802.
2. Ong, P.L.; Levitsky, I.A. Organic/IV, III-V semiconductor hybrid solar cells. *Energies* **2010**, *3*, 313–334.
3. Ho, T.; Mao, S.S.; Greif, R. The impact of cooling on cell temperature and the practical solar concentration limits for photovoltaics. *Int. J. Energy Res.* **2011**, *35*, 1250–1257.
4. He, W.; Chow, T.T.; Ji, J. Hybrid photovoltaic and thermal solar-collector designed for natural circulation of water. *Appl. Energy* **2006**, *83*, 199–210.
5. Quan, Z.H.; Li, N.J.; Zhao, Y.H. Experimental study of solar photovoltaic / thermal (PV / T) system based on flat plate heat pipe. In *Proceedings of the 2011 Asia-Pacific Power and Energy Engineering Conference*, Wuhan, China, 25–28 March 2011.
6. Yildiz, A.; Ozgener, O.; Ozgener, L. Exergetic performance assessment of solar photovoltaic cell (PV) assisted earth to air heat exchanger (EAHE) system for solar greenhouse cooling. *Energy Build.* **2011**, *43*, 3154–3160.
7. Ganesha Prasad, M.S.; Drakshayani, D.N. Studies on passive cooling techniques in dry machining. *Mater. Manuf. Process.* **2010**, *25*, 360–369.
8. Kuo, C.T.; Shin, H.Y.; Hong, H.F.; Wu, C.H.; Lee, C.D.; Lung, I.T.; Hsu, Y.T. Development of the high concentration III-V photovoltaic system at INER, Taiwan. *Renew. Energy* **2009**, *34*, 1931–1933.

9. Zhang, M.; Liu, Z.L.; Ma, G.Y.; Cheng, S.Y. The experimental study on flat plate heat pipe of magnetic working fluid. *Exp. Therm. Fluid Sci.* **2009**, *33*, 1100–1105.

10. Gillot, C.; Avenas, Y.; Cezac, N.; Poupom, G.; Schaeffer, C.; Fournier, E. Silicon heat pipes used as thermal spreaders. *IEEE Trans. Compon. Packag. Technol.* **2003**, *26*, 332–339.

11. Bai, P.F.; Tang, Y.; Tang, B.; Lu, L.S. Thermal performance of heat pipe with different micro-groove structures. *J. Cent. South Univ. Technol.* **2008**, *15*, 240–244.

12. Kempers, R.; Ewing, D.; Ching, C.Y. Effect of number of mesh layers and fluid loading on the performance of screen mesh wicked heat pipe. *Appl. Therm. Eng.* **2005**, *26*, 589–595.

13. Lin, L.; Ponnappan, R.; Leland, J. High performance miniature heat pipe. *Int. J. Heat Mass Transf.* **2002**, *45*, 3131–3142.